Published in final edited form as:
Glia. 2012 October ; 60(10): 1605–1618. doi:10.1002/glia.22381.

Autotaxin/ENPP2 Regulates Oligodendrocyte Differentiation *in vivo* in the Developing Zebrafish Hindbrain

Larra W. Yuelling[1], **Christopher T. Waggener**[1], **Fatemah S. Afshari**[1], **James A. Lister**[2], and **Babette Fuss**[1,*]

[1]Department of Anatomy and Neurobiology, Virginia Commonwealth University School of Medicine, Richmond, Virginia

[2]Department of Human and Molecular Genetics, Virginia Commonwealth University School of Medicine, Richmond, Virginia

Abstract

During development, progenitors that are committed to differentiate into oligodendrocytes, the myelinating cells of the central nervous system (CNS), are generated within discrete regions of the neuroepithelium. More specifically, within the developing spinal cord and hindbrain ventrally located progenitor cells that are characterized by the expression of the transcription factor *olig2* give temporally rise to first motor neurons and then oligodendrocyte progenitors. The regulation of this temporal neuron-glial switch has been found complex and little is known about the extrinsic factors regulating it. Our studies described here identified a zebrafish ortholog to mammalian *atx,* which displays evolutionarily conserved expression pattern characteristics. Most interestingly, *atx* was found to be expressed by cells of the cephalic floor plate during a time period when ventrally-derived oligodendrocyte progenitors arise in the developing hindbrain of the zebrafish. Knock-down of *atx* expression resulted in a delay and/or inhibition of the timely appearance of oligodendrocyte progenitors and subsequent developmental stages of the oligodendrocyte lineage. This effect of *atx* knock-down was not accompanied by changes in the number of *olig2*-positive progenitor cells, the overall morphology of the axonal network or the number of somatic abducens motor neurons. Thus, our studies identified Atx as an extrinsic factor that is likely secreted by cells from the floor plate and that is involved in regulating specifically the progression of *olig2*-positive progenitor cells into lineage committed oligodendrocyte progenitors.

Keywords

myelination; glia differentiation; CNS development; floor plate; zebrafish

INTRODUCTION

During development, oligodendrocytes, the myelinating cells of the vertebrate central nervous systems (CNS), are generated from neural progenitor cells that are located within distinct regions of the neuroepithelium (Miller, 2005; Richardson et al., 2006; Rowitch and Kriegstein, 2010). The most direct known domain of progenitor cells giving rise to ventrally-derived oligodendrocytes in the developing spinal cord and hindbrain is composed of progenitor cells that sequentially generate first motor neurons and then oligodendrocytes

*Correspondence to: Babette Fuss, Department of Anatomy and Neurobiology, Virginia Commonwealth University School of Medicine, PO BOX 980709, Richmond, VA 23298, Phone : 804 827 0826, bfuss@vcu.edu.

(Richardson et al., 2000; Rowitch et al., 2002; Wu et al., 2006) and that can be identified via the expression of the transcription factor *olig2* (Lu et al., 2002; Mukouyama et al., 2006; Park et al., 2002; Takebayashi et al., 2002; Zannino and Appel, 2009; Zhou and Anderson, 2002). Despite extensive research, however, the exact mechanisms and factors determining the timely appearance of oligodendrocyte progenitors from *olig2*-positive progenitor cells are currently not fully understood.

A well characterized factor regulating early development of both motor neurons and ventrally-derived oligodendrocyte progenitors is sonic hedgehog (Shh), which is expressed and secreted by cells of the floor plate (Jessell, 2000; Orentas and Miller, 1996; Park et al., 2004; Poncet et al., 1996; Pringle et al., 1996). The floor plate is, however, known to release extracellular factors other than Shh (Placzek and Briscoe, 2005), suggesting that it may contribute to additional developmental mechanisms, possibly including the regulation of oligodendrocyte development via a yet uncharacterized floor plate-derived signal.

In our previous studies we identified autotaxin (Atx), also known as Enpp2, phosphodiesterase-Iα/Atx or lysoPLD, as an extracellular factor that promotes differentiation of particularly the later stages of the oligodendrocytes lineage (Dennis et al., 2008; Fox et al., 2004; Fox et al., 2003; Yuelling and Fuss, 2008). More specifically, Atx was found to promote morphological maturation of differentiating oligodendrocytes via its C-terminal domain, referred to as the modulator of oligodendrocyte remodeling and focal adhesion organization (MORFO) domain. As such regulator of oligodendrocyte maturation, Atx is thought to act as an autocrine signal since it is expressed and secreted by differentiating oligodendrocytes. It is worth mentioning that while Atx has been originally thought to be a proteolytically cleavable transmembrane protein, it is now well established to represent a bona fide secretory protein (Jansen et al., 2005; Koike et al., 2006). During embryonic development, particularly during the developmental time period when ventrally-derived oligodendrocyte progenitors are generated (Pringle and Richardson, 1993; Richardson et al., 2000; Sussman et al., 2000), *atx* was found in the mouse to be expressed by cells of the floor plate (Bachner et al., 1999). This spatio-temporal expression raises the possibility that Atx may play an additional paracrine role in regulating the initial stages of oligodendrocyte development. Knock-out mice for *atx* have been generated. However, they are characterized by an early embryonic lethal phenotype due to severe vascular defects, thus rendering them uninformative with regard to a potential *in vivo* role of *atx* in regulating oligodendrocyte development (Ferry et al., 2007; Fotopoulou et al., 2010; Koike et al., 2009; Tanaka et al., 2006; van Meeteren et al., 2006).

Here, the *in vivo* role of *atx* in oligodendrocyte development was assessed using the zebrafish as a model system. The choice of the model system was based on the notion that zebrafish embryos can develop independent from a fully functional vascular system for up to seven days post fertilization (Jin et al., 2007; Ny et al., 2006; Stainier, 2001), a time frame that is sufficient for investigating oligodendrocyte development (Brosamle and Halpern, 2002; Buckley et al., 2010; Kirby et al., 2006; Park et al., 2002; Schebesta and Serluca, 2009). First, a zebrafish ortholog to mammalian *atx* was identified and found to display evolutionarily conserved expression pattern characteristics. Then, using morpholino antisense oligonucleotide-mediated gene silencing, our studies revealed that in the developing zebrafish hindbrain *atx* promotes the differentiation of oligodendrocyte progenitors from *olig2*-positive progenitor cells. Furthermore, our findings suggest that this novel functional role of *atx* occurs by a paracrine mechanism with cells of the floor plate as the most likely source for secreted Atx.

MATERIALS AND METHODS

Zebrafish Strains and Care

Wildtype embryos of the AB strain were obtained through natural matings, raised at 28.5°C and staged according to morphological criteria and hours post fertilization (hpf) (Kimmel et al., 1995).

Sequence Analysis and cDNA Cloning

Sequence data for zebrafish *atx* (ZDB-GENE-040426-1156, NM_200603.1) were obtained using NCBI's Basic Local Alignment Search Tool (BLAST; Sayers et al., 2011). Amino acid sequence alignments and phylogenic guide trees were generated using the Vector NTI software package (Invitrogen, Carlsbad, CA). The authors would like to note that while zebrafish *atx* is recorded under the gene symbol *enpp2*, the symbol *atx* will be used throughout the manuscript since this is currently the most commonly used designation.

For the generation of gene-specific cRNA probes the following plasmid constructs were used: *atx*: a 1843 bp ClaI-KpnI fragment containing the 3' 1812 bps of the 2552 bp *atx* coding region was excised from the I.M.A.G.E. clone 3816628 (Open Biosystems, Huntsville, AL) and inserted into pBluescript (Agilent Technologies/Stratagene, La Jolla, CA). *olig1* (ZDB-GENE-050107-2): a 674 bp fragment covering most of the 708 bp *olig1* coding region was amplified from zebrafish embryo RNA (3 dpf). The resulting amplification product was cloned into pBluescript. *shhb* (ZDB-GENE-980526-41): a 1990 bp fragment containing the entire *shhb* coding region was amplified from I.M.A.G.E. clone 7149635 (ATCC, Manassas, VA) and a T3 RNA polymerase binding site was introduced at the 3' end. In addition, previously described plasmid constructs were used for the following genes: *foxa1* (ZDB-GENE-990415-78): Odenthal and Nusslein-Volhard, 1998, *foxa2* (ZDB-GENE-980526-404): Strahle et al., 1993, *mbp* (ZDB-GENE-030128-2): Brosamle and Halpern, 2002, *olig2* (ZDB-GENE-030131-4013): Park et al., 2002, *sox10* (ZDB-GENE-011207-1): Dutton et al., 2001.

Whole-Mount *In Situ* Hybridization and Immunohistochemistry

Embryos were fixed in 4% paraformaldehyde in PBS overnight at 4°C and stored in methanol at −20°C for at least 1 day. Colorimetric *in situ* hybridizations using digoxigenin-labeled antisense cRNA probes were performed by standard methods (Thisse and Thisse, 2008). Fluorescent immunostainings using the anti-neurofilament M antibody RMO44 (Invitrogen, Carlsbad, CA) and the anti-Neurolin/DM-GRASP antibody Zn-8 (Developmental Studies Hybridoma Bank, Iowa City, Iowa) were performed in principle as described by Waskiewicz et al. (2001) and Zannino and Appel (2009), respectively.

In situ hybridized and immunostained embryos were imaged either as whole-mounts or cryoprotected (30% sucrose/PBS), embedded in Tissue-Tek O.C.T. Compound (Sakura Finetek, Torrance, CA) and cryosectioned (20 μm; Cryotome Cryostat; Shandon, Inc., Pittsburgh, PA). Embryos and sections of colorimetric *in situ* hybridizations were mounted in 90% glycerol/PBS. Images were acquired using either the extended focus module of the axiovision software package in combination with an Axio Observer Z.1 or SteREO Discovery.V20 microscope equipped with an AxioCam MRc digital camera (Carl Zeiss MicroImaging, Inc., Thornwood, NY) or an Olympus SZX12 stereomicroscope equipped with a DP70 digital camera (Olympus, Center Valley, PA). Fluorescently immunostained embryos were mounted in Vectashield mounting medium (Vector laboratories, Burlingame, CA) and images were acquired using a Zeiss LSM 510 META NLO laser scanning microscope (Carl Zeiss MicroImaging, Thornwood, NY). Once captured, images were imported into Adobe Photoshop and adjustments were limited to contrast, levels, color

matching settings, and cropping. For quantification of RMO44-immuno-positive pixels 2D maximum projections of confocal Z stacks of 5.66 μm optical sections were analyzed without prior image adjustments using IPLab imaging software (BioVision Technologies, Exton, PA).

Morpholino Oligonucleotide and mRNA Injections

Two antisense morpholino oligonucleotides (MOs) targeting *atx* were designed and synthesized by GeneTools (Philomath, OR) in accordance with the published zebrafish genome sequence (Ensembl entry ENSDART00000047920): *atx* TL MO (5'-TGCGTCTGGTGGCTCTCTTCCACAC-3') was designed to target the *atx* translation start site, while *atx* E2I2 MO (5'-AAGAAGCATCCTACTTTTTGAGAGC-3') was designed to target the exon 2-intron 2 splice site of *atx*. As controls, 5 base pair mismatch MOs were used: *atx* TL control MO (5'-TGCGTGTGGTGCCTGTCTTGCAGAC-3') and *atx* E2I2 control MO (5'-AACAAGGATCGTACTTTTTGACACC-3'). MOs were reconstituted in H_2O and diluted in 1× Danieau buffer (58 mM NaCl, 0.7 mM KCl,. 0.4 mM $MgSO_4$, 0.6 mM $Ca(NO_3)_2$, 5.0 mM HEPES pH 7.6). 1 nl was injected into the yolk of one- to four-cell-stage embryos. *atx* TL MO and *atx* TL control MO were injected at a concentration of 1 mg/ml, while *atx* E2I2 MO and *atx* E2I2 control MO were used at a concentration of 10 mg/ml. To confirm that phenotypes observed upon MO injections were not due to Tp53-mediated activation of cell death pathways, an often observed MO off-target effect (Gerety and Wilkinson, 2011; Robu et al., 2007), *atx* TL MO injected and uninjected embryos were immunostained at 24 hpf with an anti-cleaved caspase-3 antibody. No significant difference in the number of cleaved caspase-3-positive cells was observed (data not shown).

For mRNA rescue experiments 5′ capped and 3' polyadenylated *atx* sense RNA was synthesized from a full-length rat-derived cDNA cloned into the vector pEF/V5-His (Dennis et al., 2008) using mMessage mMachine T7 and Poly(A) Tailing kits (Life Technologies/Ambion, Grand Island, NY). 1 nl of mRNA (20 ng/μl) was injected into the yolk of one- to four-cell-stage embryos directly following the injection of the *atx* TL MO.

Western Blot Analysis

Embryos were deyolked and homogenized in lysis buffer (40 mM NaCl, 40 mM HEPES (pH 7.4), 10 mM EDTA, 0.1% SDS, 1% Triton) including the cOmplete mini protease inhibitor cocktail (Roche Diagnostics Corp., Indianapolis, IN). Lysates were centrifuged at 10,000×g for 5 min and supernatants were collected. Proteins were resolved by sodium dodecyl sulfate polyacrylamide gel electrophoresis and transferred to Immobilon-P PDVF membranes (Millipore, Billerica, MA) in principle as previously described (Fuss et al., 2000). Polyclonal anti-Atx antibodies were generated against a peptide representing amino acids 827–840 (RRTSRTYEEILALK) of the zebrafish Atx protein sequence (EZBiolab, Inc., Westfield, IN) and used at a dilution of 1:10,000. These zebrafish-specific antibodies recognized in whole zebrafish lysates protein forms with apparent molecular weights of 100 kD and 125/135 kD (Fig. 3A), which is consistent with the molecular weights described for unmodified and post-translationally modified Atx protein forms, respectively (Jansen et al., 2007; Pradere et al., 2007). In contrast, none of the alternatively spliced exon sequences found in higher vertebrates (Giganti et al., 2008) were found present in the published zebrafish genomic *atx* sequences. The binding to all of the above protein forms was inhibited by pre-incubation with the peptide used for antibody production. In addition, polyconal anti-Atx antibodies raised against a peptide representing amino acids 573–588 (KNKLEELNKRLHTKGS) of the rat Atx protein sequence (Cayman Chemical Company, Ann Arbor, MI) were used at a dilution of 1:1,000. These antibodies recognized, similar to the above anti-zebrafish Atx generated antibodies, proteins with apparent molecular weights of 100 kD and 125/135 kD (Fig. 6A). Anti-β-tubulin antibodies (1:1000; Sigma-Aldrich, St.

Louis, MO) were used for normalization. Bound primary antibodies were detected using HRP-conjugated secondary antibodies (1:10,000; Vector Laboratories, Burlingame, CA) in combination with ECL Plus Western blot detection reagents (GE Healthcare Life Sciences, Piscataway, NJ). Chemiluminescent signals were detected by exposure of photographic film (Kodak BioMax MR, Eastman Kodak Company, Rochester, NY) and quantified by densitometry using the ImageJ software package (Abramoff et al., 2004).

Quantitative RT-PCR

Total RNA samples were isolated from embryos using Trizol (Invitrogen, Carlsbad, CA) and treated with DNase using the DNA-Free kit (Applied Biosystems/Ambion, Austin, TX). Oligo(dT)-primed cDNAs were synthesized using the Superscript II RT kit (Invitrogen, Carlsbad, CA). Quantitative RT-PCR was performed on a Chromo4 (MJ Research, Inc., Waltham, MA) or CFX96 (BioRad, Hercules, CA) real-time PCR detection system using the iQ SYBR Green Supermix (BioRad, Hercules, CA). The following primer pairs were used at an annealing temperature of 58°C: *mbp* primer pair as described by Buckley et al. (2010); *plp1b* primer pair: Forward: 5'-TGCCATGCCAGGGGTTGTTTGTGGA-3' and Reverse: 5'-GGCGACCATGTAAACGAACAGGGC-3'; *cldnk* primer pair: Forward: 5'-TGGCATTTCGGCTCAAGCTCTGGA-3' and Reverse: 5'-GGTACAGACTGGGCAATGGACCTGA-3'; *olig1* primer pair: Forward: 5'-CCGGTGTAGGGGGAGCACTGCA-3' and Reverse 5-'TCCGAGCCAGCACCAGTGTCGAG-3'. *β-actin* (Buckley et al., 2010) was used as reference gene and relative expression levels were determined using the ΔΔCT method (Livak and Schmittgen, 2001). Statistical significance was determined using the one-sample *t*-test (Dalgaard, 2008; Skokal and Rohlf, 1995).

RESULTS

An Ortholog of Mammalian *atx* is Present in the Zebrafish

A zebrafish ortholog (ZDB-GENE-040426-1156, NM_200603.1) of the known rat and human *atx* mRNA sequences was identified within the ZFIN RNA/cDNA database (Bradford et al., 2011) using BLAST searches. This zebrafish ortholog is identical to the one that has been recently characterized to regulate early vascular development in the zebrafish (Yukiura et al., 2011). Translation of its open reading frame revealed an amino acid sequence with high sequence conservation compared to orthologs of other vertebrate mRNA sequences (Fig. 1; Brosamle and Halpern, 2002). In addition, amino acid sequence alignments confirmed the presence of conserved structure-function domains within zebrafish Atx, namely two somatomedin B-like domains, a catalytic lysoPLD domain and a nuclease-like domain entailing a single EF hand-like motif (Supplemental Fig. S1; Gijsbers et al., 2003; Masse et al., 2010; Moolenaar, 2002; Murata et al., 1994; Narita et al., 1994; Tokumura et al., 2002; Umezu-Goto et al., 2002; Yuelling and Fuss, 2008).

The human and mouse *atx* genes span 27 exons and give rise to at least three protein isoforms, Atxα, Atxβ and Atxγ, due to alternative splicing of exons 12 and 21 (Giganti et al., 2008). The physiological relevance for these different isoforms of *atx*, however, is currently unknown. Out of these Atx protein isoforms, Atxβ, which lacks exons 12 and 21, is the only protein isoform represented by the zebrafish *atx* gene identified and appears, therefore, to be evolutionarily the oldest of the known Atx isoforms.

In the teleost fish lineage, whole-genome duplications occurred subsequent to its divergence from mammals, thus generating co-orthologs to many single mammalian genes (Ohno et al., 1968; Postlethwait et al., 2004; Postlethwait, 2007; Taylor et al., 2003). Using the Ensembl genome browser (Flicek et al., 2011), two zebrafish *atx* genes with a coding region of 99.6%

amino acid sequence identity were identified in the most recent assembly (Zv9; http://www.sanger.ac.uk/Projects/D_rerio/). These two *atx* genes are not located on different linkage groups but next to each other on chromosome 16. Thus, they are likely either a result of a tandem rather than a large scale genome duplication event, or merely represent an inaccuracy in the assembly. Most importantly, based on the sequence information available and the high sequence identity between the two *atx* genes, all probes used in the present study recognize and/or affect the products of both genes and are referred to here as the zebrafish ortholog to mammalian *atx*.

In the Developing Zebrafish *atx* Displays Expression Pattern Characteristics that are Conserved between Different Vertebrate Species

Detailed developmental *atx* expression profiles have so far been described in the mouse, chicken and frog (Bachner et al., 1999; Masse et al., 2010; Ohuchi et al., 2007). While species-specific expression variations exist, evolutionarily conserved *atx* expression does occur for example in the developing extremities (limb or fin buds) and jaw (branchial and pharyngeal arches). To assess the extent to which *atx* may be expressed in homologous structures located within the anterior part of the developing zebrafish, whole-mount *in situ* hybridizations were performed. In these studies, *atx* mRNA was first detected at 36 hpf. At all developmental ages analyzed (36–72 hpf), *atx* mRNA was found to be present in the pectoral fin buds and the pharyngeal arches (Fig. 2A). From lateral views, *atx* mRNA was at 60 and 72 hpf also detectable in a structure resembling the trabeculae cranii, a component of the developing neurocranium and thus part of the head mesenchyme (Fig. 2A). In support of an evolutionarily conserved expression and/or function, cavities in the head mesenchyme have been noted as a characteristic phenotype in *atx* knock-out mice (Koike et al., 2010). In addition, *atx* mRNA was detected in the developing head vasculature (Fig. 2A, not marked), which is consistent with recently published data (Yukiura et al., 2011) and the expression of *atx* in at least some types of blood vessels in other vertebrate species (Hoelzinger et al., 2005; Kanda et al. 2008; Masse et al. 2010; Ohuchi et al. 2007). Most interestingly, prominent expression of *atx* in the CNS was noted in the cephalic floor plate (Fig. 2B). A similar expression of *atx* in the floor plate and/or ventral spinal cord/hindbrain has been observed in all species so far analyzed with the exception of the chicken.

Taken together, the above data demonstrate that evolutionarily conserved features can be identified in *atx*'s developmental expression pattern in the zebrafish. These include an expression of *atx* by cells of the cephalic floor plate. Intriguingly, this expression coincides temporally with the appearance of differentiating oligodendrocytes in the developing hindbrain (Brosamle and Halpern, 2002; Buckley et al., 2010; Zannino and Appel, 2009).

Knock-down of *atx* Expression Delays and/or Inhibits the Appearance of Differentiating Oligodendrocytes in the Developing Zebrafish Hindbrain

The above described prominent cephalic floor plate expression of *atx* during a time period critical for oligodendrocyte development, prompted us to investigate whether knock-down of *atx* expression affects oligodendrocyte differentiation in the developing zebrafish hindbrain. In light of the known defects in vascular development upon knock-down of *atx* expression (Yukiura et al., 2011), it is of note that the vasculature is dispensable for the formation and maintenance of neuronal structures within the developing hindbrain for up to 72 hpf (Ulrich et al., 2011). However, complete knock-down of *atx* expression has been shown to cause edema in the head region, which could potentially affect CNS development (Yukiura et al., 2011). Thus, we felt it important to titrate antisense morpholino oligonucleotides to a concentration at which Atx protein levels were significantly reduced, while embryos lacked a gross morphological phenotype including head edema. Based on these criteria, we opted for conditions under which both an anti-*atx* translation blocking (*atx*

TL MO) and an anti-*atx* splice site targeted (*atx* E2I2 MO) morpholino oligonucleotide yielded Atx protein levels of about 40–50% of control levels (Fig. 3).

In *atx* knock-out mice, severe cranial neural tube defects have been described to occur in addition to vascular defects (Fotopoulou et al., 2010; Koike et al., 2011; van Meeteren et al., 2006). These neural tube defects may have developed at least in part independently from any vascular defects. Thus, to ensure that our *atx* knock-down conditions did not significantly affect the establishment of the axonal network within the developing hindbrain, whole-mount immunostainings were performed using the RMO44 antibody. This antibody recognizes a neurofilament protein strongly expressed in zebrafish reticulospinal neurons (Feng et al., 2010; Kimmel et al., 1985; Waskiewicz et al., 2001). As shown in Fig. 4, no effect on the overall morphology of the RMO44-immuno-positive axonal network was observed upon knock-down of *atx* expression.

To assess the effect of knock-down of *atx* expression on the timely appearance of differentiating oligodendrocytes, whole-mount *in-situ* hybridizations were performed. In these studies embryos were analyzed at 66 hpf, a time point at which *atx* expression appeared prominent in the cephalic floor plate (Fig. 2) but was not detectable in differentiating oligodendrocytes (data not shown). First, the expression of *myelin basic protein* (*mbp*), a gene that is expressed by differentiating and myelinating oligodendrocytes and whose mRNA is not restricted to the cytoplasm but transported into cellular processes (Brosamle and Halpern, 2002), was investigated. As shown in Fig. 5A–C, there was a significant reduction in the number of *mbp*-positive oligodendrocytes in the developing hindbrain upon knock-down of *atx* expression. A similar reduction was observed for both anti-*atx* morpholino oligonucleotides (compare Fig. 5B, C left graphs with 5B, C right graphs). This effect on *mbp* expression in the CNS was much more dramatic than any effect noticed in the peripheral nervous system (see lateral line in Fig. 5A). The reduction in the number of *mbp*-positive oligodendrocytes was also associated with a significant reduction in *mbp* mRNA levels (Fig. 5D), suggesting that mRNA levels of oligodendrocyte-enriched genes provide a reliable measure for assessing the appearance of differentiating oligodendrocytes. This idea is consistent with previous findings (Buckley et al., 2010). To assess the extent to which the effect of *atx* knock-down may be specific for *mbp* expression, the mRNA levels for two additional genes enriched in differentiating oligodendrocytes were determined, namely *proteolipid protein* (*plp1b*) and *claudin K* (*cldnk*) (Brosamle and Halpern, 2002; Munzel et al., 2012; Takada and Appel, 2010). The mRNA levels for both genes were found to be significantly reduced (Fig. 5E, F).

To further confirm the specificity of the phenotype seen upon knock-down of *atx* expression, mRNA rescue experiments were performed. In these experiments, a rat-derived synthetic *atx* mRNA was used since translation from this mRNA is not affected by the anti-*atx* translation blocking morpholino oligonucleotide. As shown in Fig. 6A, Atx protein levels were noticeably increased at 48 hpf after co-injection of the synthetic *atx* mRNA with the *atx* TL MO. Importantly, *cldnk* mRNA levels, as a measure for the appearance of differentiating oligodendrocytes, were found to be similar to control levels (Fig. 6B), thus demonstrating a restoration of the wild-type phenotype. No such restoration was observed when a beta-galactosidase encoding synthetic mRNA was co-injected with the *atx* TL MO (data not shown).

For a better evaluation of the persistence of the phenotype seen upon knock-down of *atx* expression, the number of embryos with normal and reduced/absent *mbp* expression in the hindbrain was determined at 72 hpf. As shown in Fig. 6C, there was a significant decrease in the number of embryos with normal *mbp* expression and a concomitant significant increase

in the number of embryos with reduced/absent *mbp* expression. The extent of decrease/increase was comparable to the one seen at 66 hpf (compare Fig. 6C with Fig. 5B).

Taken together, the above data demonstrate that a reduction in *atx* expression significantly delays and/or inhibits the appearance of differentiating oligodendrocytes in the developing hindbrain, and they suggest that this delay and/or inhibition is not due to gross morphological defects in the establishment of the axonal network.

Knock-down of *atx* Expression Delays and/or Inhibits the Appearance of Oligodendrocyte Progenitors in the Developing Zebrafish Hindbrain

The above data raised the possibility that the effects observed on differentiating oligodendrocytes may have been a result of an effect on the developmental lineage progression of early oligodendrocyte progenitors into differentiating oligodendrocytes that is at much earlier stages than previously observed. To investigate this possibility, whole-mount *in situ* hybridizations were performed using a probe specific for the transcription factor *olig1*, which in the developing zebrafish is expressed by oligodendrocyte progenitors. As shown in Fig. 7, knock-down of *atx* expression led to a significant reduction in the number of *olig1*-positive cells and in the level of *olig1* mRNA. The reduction in the number of *olig1*-positive cells was not found associated with a significant increase in cell death as assessed by immunostaining using an antibody specific for activated caspase-3 (data not shown). Furthermore, *olig1* expression has been described to only partially overlap with the expression of the myelin genes *mbp* and *plp1b* at a developmental age similar to the one used here (Li et al., 2007; Schebesta and Serluca 2009). Thus, if the effect of *atx* knock-down were specific to only the later stages of the oligodendrocyte lineage, a much less pronounced effect on *olig1* mRNA levels would be expected. In fact, the reduction in *olig1* mRNA levels seen upon knock-down of *atx* expression (43.31 ± 4.19 %; Fig. 7) was comparable to the reduction in *mbp* (48.31 ± 11.88%, Fig. 5), *plp1b* (58.07 ± 4.57%, Fig. 5) and *cldnk* (52.34 ± 3.86%, Fig. 5) mRNA levels. Thus, the above data demonstrate that knock-down of *atx* expression delays and/or inhibits not only the appearance of differentiating oligodendrocytes but also oligodendrocyte progenitors.

Knock-down of *atx* Expression Delays and/or Inhibits the Differentiation of Oligodendrocyte Progenitors from *olig2*-positive Progenitor Cells in the Developing Zebrafish Hindbrain

To further define the developmental stage at which knock-down of *atx* expression affects the developmental progression of cells of the oligodendrocyte lineage, zebrafish embryos were analyzed at 48 hpf. At this developmental time point oligodendrocyte progenitors expressing the transcription factor *sox10* begin to differentiate in the developing hindbrain from *olig2*-positive progenitor cells (Zannino and Appel, 2009). As shown in Fig. 8A,B, knock-down of *atx* expression resulted in a reduction in the number of embryos with normal expression of *sox10* in the developing hindbrain. Conversely, the number of embryos with reduced or absent expression of *sox10* in the developing hindbrain was increased. No change in the expression of *sox10* was noted in the otic vesicles. In contrast to the effects seen on *sox10*-positve oligodendrocyte progenitors, the number of *olig2*-positive cells remained unchanged (Fig. 8C,D). Thus, knock-down of *atx* expression affects in the developing hindbrain the differentiation of *olig2*-positive progenitor cells into cells of the oligodendrocyte lineage.

It has been shown previously that in the developing zebrafish hindbrain *olig2*-positive progenitor cells that are located within rhombomere r5 and r6 cell clusters can give rise to not only hindbrain oligodendrocyte progenitors but also somatic abducens motor neurons (Zannino and Appel, 2009). Thus, *atx* may be regulating not only the differentiation of oligodendrocyte progenitors from *olig2*-positive progenitor cells but also the differentiation

of somatic abducens motor neurons. To test this idea, we used the Zn-8 antibody, which recognizes Neurolin/DM-Grasp and thus somatic abducens motor neurons (Chandrasekhar et al., 1997; Kanki et al., 1994; Trevarrow et al., 1990). As shown in Fig. 9, no significant change in the number of Zn-8-immuno-positive somatic abducens motor neurons was detected upon knock-down of *atx* expression.

Taken together, the above data demonstrate that knock-down of *atx* expression delays and/or inhibits specifically the differentiation of oligodendrocyte progenitors from *olig2*-positive progenitor cells while not significantly affecting the differentiation of somatic abducens motor neurons.

DISCUSSION

The data presented here demonstrate that the zebrafish ortholog to mammalian *atx* displays evolutionarily conserved expression pattern characteristics. These include an expression of *atx* in the developing extremities and jaw. Most prominent expression in the CNS of the anterior embryo was noted in the cephalic floor plate coinciding temporally with the time period during which cells of the oligodendrocyte lineage are generated. Antisense morpholino oligonucleotide-mediated knock-down of *atx* expression revealed a functional role of *atx* in regulating early development of cells of the oligodendrocyte lineage in the developing hindbrain, without affecting the number of *olig2*-positive progenitor cells, the overall morphology of the axonal network or the differentiation of somatic abducens motor neurons. This novel functional property of *atx* is likely mediated by a paracrine mechanism and via the expression and secretion of Atx by cells of the cephalic floor plate.

In our previous studies using rodent oligodendrocytes and cell culture systems, the effects of Atx were characterized for later stages of the oligodendrocyte lineage and found to be most likely mediated by an autocrine mechanism (Dennis et al., 2008; Fox et al., 2004). Antisense morpholino oligonucleotide-mediated effects in the zebrafish have in some cases been found penetrant for up to seven days (Rinner et al., 2005; Seiler et al., 2005; van der Sar et al., 2002). Initial analysis, however, suggests that in the case of the titrated anti-*atx* morpholino oligonucleotides, Atx protein levels are almost normal at about 3 dpf, thus precluding a meaningful analysis at later developmental stages. More sophisticated experimental paradigms will thus be necessary to determine whether the effects of Atx seen in the rodent system also apply to the zebrafish.

Two functionally active sites have been described for Atx, namely the MORFO domain and the catalytic lysoPLD domain. In our previous studies we demonstrated that it is the MORFO domain that mediates morphological maturation of differentiating oligodendrocytes (Dennis et al., 2008; Fox et al., 2004; Yuelling and Fuss, 2008). Atx is, however, better known for its catalytic lysoPLD activity and the generation of the lipid signaling molecule lysophosphatidic acid (LPA) (Liu et al., 2009; Moolenaar, 2002; Nakanaga et al., 2010; Samadi et al., 2011; Tokumura et al., 2002; Umezu-Goto et al., 2002; van Meeteren and Moolenaar, 2007). As an extracellular lysophospholipid, LPA exerts its functions through interactions with a family of G protein-coupled receptors, the family of LPA receptors (Chun et al., 2010; Lin et al., 2009; Yanagida and Ishii, 2011). Orthologs for at least some of the known mammalian LPA receptors have been identified in the zebrafish (Lee et al., 2008; Yukiura et al., 2011), and cells of the oligodendrocyte lineage have long been known to express a variety of LPA receptors (Dawson et al., 2003; Nogaroli et al., 2009; Stankoff et al., 2002; Weiner et al., 1998; Yu et al., 2004). In addition, LPA receptors have been functionally implicated in the regulation of early CNS development (Choi et al., 2008; Estivill-Torrus et al., 2008; Fukushima et al., 2007; Hecht et al., 1996; Kingsbury et al., 2003; Kingsbury et al., 2004). However, little is currently known about the role of LPA

signaling for early glial and in particular oligodendroglial development. In support of a potential role of LPA in gliogenesis, LPA has been shown to promote the differentiation of oligodendrocytes from neural stem/progenitor cells, at least under certain cell culture conditions (Cui and Qiao, 2007; Pitson and Pebay, 2009; Svetlov et al., 2004). Such effects of LPA may be mediated by autocrine as well as paracrine mechanisms. Atx has traditionally been regarded as an autocrine factor. However, there is increasing evidence for paracrine roles, all of which have so far been attributed to the synthesis of LPA (Ferry et al., 2003; Hoelzinger et al., 2008; Kanda et al., 2008). Such paracrine roles of Atx are further facilitated by slow catalytic kinetics and a predicted mobility of Atx-lipid complexes up to a distance of approximately 65 μm (Saunders et al., 2011). With regard to our findings, all the above data point toward a primary role of Atx's catalytic lysoPLD activity, rather than its MORFO domain, in stimulating the progression of *olig2*-positive progenitor cells into oligodendrocyte progenitors in a paracrine, rather than autocrine, fashion.

It has been well established in the spinal cord that there are ventral as well as dorsal origins for cells of the oligodendrocyte lineage (Miller, 2005; Richardson et al., 2006). While less well characterized, the same appears to be true for hindbrain oligodendrocytes (Davies and Miller, 2001; Vallstedt et al., 2005; Zannino and Appel, 2009). The molecular mechanisms regulating the development of ventrally- and dorsally-derived oligodendrocytes have been shown to involve different extracellular signals (Bilican et al., 2008; Cai et al., 2005; Fogarty et al., 2005; Langseth et al., 2010; Vallstedt et al., 2005). Based on our findings, one would predict that at least in the developing zebrafish, Atx's role in regulating early oligodendrocyte development may be restricted to ventrally-derived oligodendrocytes. In homology, the same would apply to the developing mouse, where *atx* has been described expressed by cells of the floor plate (Bachner et al., 1999; Ohuchi et al., 2007). In contrast, *atx* was found expressed in the alar plate in the chicken (Ohuchi et al., 2007), and it is thus tempting to speculate that in the chicken *atx* may play a functional role in regulating the development of dorsally-derived oligodendrocytes.

Ventrally-derived oligodendrocytes arise in the developing spinal cord and hindbrain from *olig2*-positive progenitor cells that are located within a progenitor niche that gives rise first to motor neurons and then to oligodendrocytes. The regulation of this neuron-glial switch has been found complex involving cell intrinsic factors as well as extracellular signaling factors (for reviews see: Richardson et al., 2000; Rowitch, 2004; Rowitch et al., 2002). In this regard, our data identify *atx* as an attractive novel candidate for an extracellular signaling factor involved in promoting the generation of cells of the oligodendrocyte lineage from *olig2*-positive progenitor cells.

Supplementary Material

Refer to Web version on PubMed Central for supplementary material.

Acknowledgments

The authors would like to thank Bruce Appel and Marnie Halpern for generously providing reagents and invaluable discussions. The authors also thank Gregory Walsh for helpful advice. Microscopy was performed at the VCU Department of Anatomy and Neurobiology Microscopy Facility, supported, in part, with funding from NIH-NINDS Center Core grant (5P30NS047463). The monoclonal antibody Zn-8, developed by Bill Trevarrow, was obtained from the Developmental Studies Hybridoma Bank developed under the auspices of the NICHD and maintained by the Department of Biology at The University of Iowa. This work was supported by grants from the NIH-NINDS (B.F.) and the National Multiple Sclerosis Society (B.F.).

REFERENCES

Abramoff M, Magelhaes P, Ram S. Image Processing with image. Journal of Biophotonics Int. 2004; 11:36–42.

Bachner D, Ahrens M, Betat N, Schroder D, Gross G. Developmental expression analysis of murine autotaxin (ATX). Mech Dev. 1999; 84:121–125. [PubMed: 10473125]

Bilican B, Fiore-Heriche C, Compston A, Allen ND, Chandran S. Induction of Olig2 precursors by FGF involves BMP signalling blockade at the Smad level. PLoS One. 2008; 3:e2863. [PubMed: 18682850]

Bradford Y, Conlin T, Dunn N, Fashena D, Frazer K, Howe DG, Knight J, Mani P, Martin R, Moxon SA, et al. ZFIN: enhancements and updates to the Zebrafish Model Organism Database. Nucleic Acids Res. 2011; 39(Database issue):D822–D829. [PubMed: 21036866]

Brosamle C, Halpern ME. Characterization of myelination in the developing zebrafish. Glia. 2002; 39:47–57. [PubMed: 12112375]

Buckley CE, Marguerie A, Alderton WK, Franklin RJM. Temporal dynamics of myelination in the zebrafish spinal cord. Glia. 2010; 58:802–812. [PubMed: 20140960]

Cai J, Qi Y, Hu X, Tan M, Liu Z, Zhang J, Li Q, Sander M, Qiu M. Generation of oligodendrocyte precursor cells from mouse dorsal spinal cord independent of Nkx6 regulation and Shh signaling. Neuron. 2005; 45:41–53. [PubMed: 15629701]

Chandrasekhar A, Moens CB, Warren JT Jr, Kimmel CB, Kuwada JY. Development of branchiomotor neurons in zebrafish. Development. 1997; 124:2633–2644. [PubMed: 9217005]

Choi JW, Lee CW, Chun J. Biological roles of lysophospholipid receptors revealed by genetic null mice: an update. Biochim Biophys Acta. 2008; 1781:531–539. [PubMed: 18407842]

Chun J, Hla T, Lynch KR, Spiegel S, Moolenaar WH. International Union of Basic and Clinical Pharmacology. LXXVIII. Lysophospholipid receptor nomenclature. Pharmacol. 2010; 62:579–587.

Cui HL, Qiao JT. Effect of lysophosphatidic acid on differentiation of embryonic neural stem cells into neuroglial cells in rats in vitro. Sheng Li Xue Bao. 2007; 59(6):759–764. [PubMed: 18157468]

Dalgaard, P., editor. Introductory Statistics with R. 2nd ed.. New York: Springer; 2008.

Davies JE, Miller RH. Local sonic hedgehog signaling regulates oligodendrocyte precursor appearance in multiple ventricular zone domains in the chick metencephalon. Dev Biol. 2001; 233:513–525. [PubMed: 11336511]

Dawson J, Hotchin N, Lax S, Rumsby M. Lysophosphatidic acid induces process retraction in CG-4 line oligodendrocytes and oligodendrocyte precursor cells but not in differentiated oligodendrocytes. J Neurochem. 2003; 87:947–957. [PubMed: 14622125]

Dennis J, White MA, Forrest AD, Yuelling LM, Nogaroli L, Afshari FS, Fox MA, Fuss B. Phosphodiesterase-Ialpha/autotaxin's MORFO domain regulates oligodendroglial process network formation and focal adhesion organization. Mol Cell Neurosci. 2008; 37:412–424. [PubMed: 18164210]

Dutton KA, Pauliny A, Lopes SS, Elworthy S, Carney TJ, Rauch J, Geisler R, Haffter P, Kelsh RN. Zebrafish colourless encodes sox10 and specifies non-ectomesenchymal neural crest fates. Development. 2001; 128:4113–4125. [PubMed: 11684650]

Estivill-Torrus G, Llebrez-Zayas P, Matas-Rico E, Santin L, Pedraza C, De Diego I, Del Arco I, Fernandez-Llebrez P, Chun J, De Fonseca FR. Absence of LPA1 signaling results in defective cortical development. Cereb Cortex. 2008; 18:938–950. [PubMed: 17656621]

Feng L, Hernandez RE, Waxman JS, Yelon D, Moens CB. Dhrs3a regulates retinoic acid biosynthesis through a feedback inhibition mechanism. Dev Biol. 2010; 338:1–14. [PubMed: 19874812]

Ferry G, Giganti A, Coge F, Bertaux F, Thiam K, Boutin JA. Functional invalidation of the autotaxin gene by a single amino acid mutation in mouse is lethal. FEBS Lett. 2007; 581:3572–3578. [PubMed: 17628547]

Ferry G, Tellier E, Try A, Gres S, Naime I, Simon MF, Rodriguez M, Boucher J, Tack I, Gesta S, et al. Autotaxin is released from adipocytes, catalyzes lysophosphatidic acid synthesis, and activates preadipocyte proliferation. Up-regulated expression with adipocyte differentiation and obesity. J Biol Chem. 2003; 278:18162–18169. [PubMed: 12642576]

Flicek P, Amode MR, Barrell D, Beal K, Brent S, Chen Y, Clapham P, Coates G, Fairley S, Fitzgerald S, et al. Ensembl 2011. Nucleic. 2011; 39(Database issue):D800–D806.

Fogarty M, Richardson WD, Kessaris N. A subset of oligodendrocytes generated from radial glia in the dorsal spinal cord. Development. 2005; 132:1951–1959. [PubMed: 15790969]

Fotopoulou S, Oikonomou N, Grigorieva E, Nikitopoulou I, Paparountas T, Thanassopoulou A, Zhao Z, Xu Y, Kontoyiannis DL, Remboutsika E, et al. ATX expression and LPA signalling are vital for the development of the nervous system. Dev Biol. 2010; 339:451–464. [PubMed: 20079728]

Fox MA, Alexander JK, Afshari FS, Colello RJ, Fuss B. Phosphodiesterase-I alpha/autotaxin controls cytoskeletal organization and FAK phosphorylation during myelination. Mol Cell Neurosci. 2004; 27:140–150. [PubMed: 15485770]

Fox MA, Colello RJ, Macklin WB, Fuss B. Phosphodiesterase-Ialpha/autotaxin: a counteradhesive protein expressed by oligodendrocytes during onset of myelination. Mol Cell Neurosci. 2003; 23:507–519. [PubMed: 12837632]

Fukushima N, Shano S, Moriyama R, Chun J. Lysophosphatidic acid stimulates neuronal differentiation of cortical neuroblasts through the LPA1-G(i/o) pathway. Neurochem Int. 2007; 50:302–307. [PubMed: 17056154]

Fuss B, Mallon B, Phan T, Ohlemeyer C, Kirchhoff F, Nishiyama A, Macklin WB. Purification and analysis of *in vivo*-differentiated oligodendrocytes expressing the green fluorescent protein. Dev Biol. 2000; 218:259–274. [PubMed: 10656768]

Gerety SS, Wilkinson DG. Morpholino artifacts provide pitfalls and reveal a novel role for pro-apoptotic genes in hindbrain boundary development. Dev. 2011; 350:279–289.

Giganti A, Rodriguez M, Fould B, Moulharat N, Coge F, Chomarat P, Galizzi JP, Valet P, Saulnier-Blache JS, Boutin JA, et al. Murine and human autotaxin alpha, beta, and gamma isoforms: gene organization, tissue distribution, and biochemical characterization. J Biol Chem. 2008; 283:7776–7789. [PubMed: 18175805]

Gijsbers R, Aoki J, Arai H, Bollen M. The hydrolysis of lysophospholipids and nucleotides by autotaxin (NPP2) involves a single catalytic site. FEBS Lett. 2003; 5383:60–64. [PubMed: 12633853]

Hecht JH, Weiner JA, Post SR, Chun J. Ventricular zone gene-1 (vzg-1) encodes a lysophosphosphatidic acid receptor expressed in neurogenic regions of the developing cerebral cortex. J Cell Biol. 1996; 135:1071–1083. [PubMed: 8922387]

Hoelzinger DB, Mariani L, Weis J, Woyke T, Berens TJ, McDonough WS, Sloan A, Coons SW, Berens ME. Gene expression profile of glioblastoma multiforme invasive phenotype points to new therapeutic targets. Neoplasia. 2005; 7:7–16. [PubMed: 15720813]

Hoelzinger DB, Nakada M, Demuth T, Rosensteel T, Reavie LB, Berens ME. Autotaxin: a secreted autocrine/paracrine factor that promotes glioma invasion. J Neurooncol. 2008; 86:297–309. [PubMed: 17928955]

Jansen S, Stefan C, Creemers JW, Waelkens E, Van Eynde A, Stalmans W, Bollen M. Proteolytic maturation and activation of autotaxin (NPP2), a secreted metastasis-enhancing lysophospholipase D. J Cell Sci. 2005; 118:3081–3089. [PubMed: 15985467]

Jansen S, Callewaert N, Dewerte I, Andries M, Ceulemans H, Bollen M. An essential oligomannosidic glycan chain in the catalytic domain of autotaxin, a secreted lysophospholipase-D. J Biol Chem. 2007; 282:11084–11091. [PubMed: 17307740]

Jessell TM. Neuronal specification in the spinal cord: inductive signals and transcriptional codes. Nat Rev Genet. 2000; 1:20–29. [PubMed: 11262869]

Jin SW, Herzog W, Santoro MM, Mitchell TS, Frantsve J, Jungblut B, Beis D, Scott IC, D'Amico LA, Ober EA, et al. A transgene-assisted genetic screen identifies essential regulators of vascular development in vertebrate embryos. Dev Biol. 2007; 307:29–42. [PubMed: 17531218]

Kanda H, Newton R, Klein R, Morita Y, Gunn MD, Rosen SD. Autotaxin, an ectoenzyme that produces lysophosphatidic acid, promotes the entry of lymphocytes into secondary lymphoid organs. Nat Immunol. 2008; 9:415–423. [PubMed: 18327261]

Kanki JP, Chang S, Kuwada JY. The molecular cloning and characterization of potential chick DM-GRASP homologs in zebrafish and mouse. J Neurobiol. 1994; 25:831–845. [PubMed: 8089660]

Kimmel CB, Ballard WW, Kimmel SR, Ullmann B, Schilling TF. Stages of embryonic development of the zebrafish. Dev Dyn. 1995; 203:253–310. [PubMed: 8589427]

Kimmel CB, Metcalfe WK, Schabtach E. T reticular interneurons: a class of serially repeating cells in the zebrafish hindbrain. J Comp Neurol. 1985; 233:365–376. [PubMed: 3980775]

Kingsbury MA, Rehen SK, Contos JJ, Higgins CM, Chun J. Non-proliferative effects of lysophosphatidic acid enhance cortical growth and folding. Nat Neurosci. 2003; 6:1292–1299. [PubMed: 14625558]

Kingsbury MA, Rehen SK, Ye X, Chun J. Genetics and cell biology of lysophosphatidic acid receptor-mediated signaling during cortical neurogenesis. J Cell Biochem. 2004; 92:1004–1012. [PubMed: 15258921]

Kirby BB, Takada N, Latimer AJ, Shin J, Carney TJ, Kelsh RN, Appel B. In vivo time-lapse imaging shows dynamic oligodendrocyte progenitor behavior during zebrafish development. Nat Neurosci. 2006; 9:1506–1511. [PubMed: 17099706]

Koike S, Keino-Masu K, Masu M. Deficiency of autotaxin/lysophospholipase D results in head cavity formation in mouse embryos through the LPA receptor-Rho-ROCK pathway. Biochem Biophys Res Commun. 2010; 400:66–71. [PubMed: 20692235]

Koike S, Keino-Masu K, Ohto T, Masu M. The N-terminal hydrophobic sequence of autotaxin (ENPP2) functions as a signal peptide. Genes Cells. 2006; 11:133–142. [PubMed: 16436050]

Koike S, Keino-Masu K, Ohto T, Sugiyama F, Takahashi S, Masu M. Autotaxin/lysophospholipase D-mediated lysophosphatidic acid signaling is required to form distinctive large lysosomes in the visceral endoderm cells of the mouse yolk sac. J Biol Chem. 2009; 284:33561–33570. [PubMed: 19808661]

Koike S, Yutoh Y, Keino-Masu K, Noji S, Masu M, Ohuchi H. Autotaxin is required for the cranial neural tube closure and establishment of the midbrain-hindbrain boundary during mouse development. Dev Dyn. 2011; 240:413–421. [PubMed: 21246658]

Langseth AJ, Munji RN, Choe Y, Huynh T, Pozniak CD, Pleasure SJ. Wnts influence the timing and efficiency of oligodendrocyte precursor cell generation in the telencephalon. J Neurosci. 2010; 6:13367–13372. [PubMed: 20926663]

Lee SJ, Chan TH, Chen TC, Liao BK, Hwang PP, Lee H. LPA1 is essential for lymphatic vessel development in zebrafish. FASEB J. 2008; 22:3706–3715. [PubMed: 18606866]

Li H, Lu Y, Smith HK, Richardson WD. Olig1 and Sox10 interact synergistically to drive myelin basic protein transcription in oligodendrocytes. J Neurosci. 2007; 27:14375–14382. [PubMed: 18160645]

Lin ME, Herr DR, Chun J. Lysophosphatidic acid (LPA) receptors: signaling properties and disease relevance. Prostaglandins Other Lipid Mediat. 2009; 91:130–138. [PubMed: 20331961]

Liu S, Murph M, Panupinthu N, Mills GB. ATX-LPA receptor axis in inflammation and cancer. Cell Cycle. 2009; 8:3695–3701. [PubMed: 19855166]

Livak KJ, Schmittgen TD. Analysis of relative gene expression data using real-time quantitative PCR and the 2(−Delta Delta C(T)) Method. Methods. 2001; 25:402–408. [PubMed: 11846609]

Lu QR, Sun T, Zhu Z, Ma N, Garcia M, Stiles CD, Rowitch DH. Common developmental requirement for Olig function indicates a motor neuron/oligodendrocyte connection. Cell. 2002; 109:75–86. [PubMed: 11955448]

Masse K, Bhamra S, Allsop G, Dale N, Jones EA. Ectophosphodiesterase/nucleotide phosphohydrolase (Enpp) nucleotidases: cloning, conservation and developmental restriction. Int J Dev Biol. 2010; 54:181–193. [PubMed: 19598106]

Miller RH. Dorsally derived oligodendrocytes come of age. Neuron. 2005; 45:1–3. [PubMed: 15629694]

Moolenaar WH. Lysophospholipids in the limelight: autotaxin takes center stage. J Cell Biol. 2002; 158:197–199. [PubMed: 12135981]

Mukouyama YS, Deneen B, Lukaszewicz A, Novitch BG, Wichterle H, Jessell TM, Anderson DJ. Olig2+ neuroepithelial motoneuron progenitors are not multipotent stem cells in vivo. Proc Natl Acad Sci U S A. 2006; 103:1551–1556. [PubMed: 16432183]

Munzel EJ, Schaefer K, Obirei B, Kremmer E, Burton EA, Kuscha V, Becker CG, Brosamle C, Williams A, Becker T. Claudin k is specifically expressed in cells that form myelin during

development of the nervous system and regeneration of the optic nerve in adult zebrafish. Glia. 2012; 60:253–270. [PubMed: 22020875]

Murata J, Lee HY, Clair T, Krutzsch HC, Arestad AA, Sobel ME, Liotta LA, Stracke ML. cDNA cloning of the human tumor motility-stimulating protein, autotaxin, reveals a homology with phosphodiesterases. J Biol Chem. 1994; 269:30479–30484. [PubMed: 7982964]

Nakanaga K, Hama K, Aoki J. Autotaxin--an LPA producing enzyme with diverse functions. J Biochem. 2010; 148:13–24. [PubMed: 20495010]

Narita M, Goji J, Nakamura H, Sano K. Molecular cloning, expression, and localization of a brain-specific phosphodiesterase I/nucleotide pyrophosphatase (PD-I alpha) from rat brain. J Biol Chem. 1994; 269:28235–28242. [PubMed: 7961762]

Nogaroli L, Yuelling LM, Dennis J, Gorse K, Payne SG, Fuss B. Lysophosphatidic acid can support the formation of membranous structures and an increase in MBP mRNA levels in differentiating oligodendrocytes. Neurochem Res. 2009; 34:182–193. [PubMed: 18594965]

Ny A, Autiero M, Carmeliet P. Zebrafish and Xenopus tadpoles: small animal models to study angiogenesis and lymphangiogenesis. Exp Cell Res. 2006; 312:684–693. [PubMed: 16309670]

Odenthal J, Nusslein-Volhard C. fork head domain genes in zebrafish. Dev Genes Evol. 1998; 208:245–258. [PubMed: 9683740]

Ohno S, Wolf U, Atkins NB. Evolution from fish to mammals by gene duplication. Hereditas. 1968; 59:169–187. [PubMed: 5662632]

Ohuchi H, Hayashibara Y, Matsuda H, Onoi M, Mitsumori M, Tanaka M, Aoki J, Arai H, Noji S. Diversified expression patterns of autotaxin, a gene for phospholipid-generating enzyme during mouse and chicken development. Dev Dyn. 2007; 236:1134–1143. [PubMed: 17366625]

Orentas DM, Miller RH. The origin of spinal cord oligodendrocytes is dependent on local influences from the notochord. Dev Biol. 1996; 177:43–53. [PubMed: 8660875]

Park HC, Mehta A, Richardson JS, Appel B. olig2 is required for zebrafish primary motor neuron and oligodendrocyte development. Dev Biol. 2002; 248:356–368. [PubMed: 12167410]

Park HC, Shin J, Appel B. Spatial and temporal regulation of ventral spinal cord precursor specification by Hedgehog signaling. Development. 2004; 131:5959–5969. [PubMed: 15539490]

Pitson SM, Pebay A. Regulation of stem cell pluripotency and neural differentiation by lysophospholipids. Neurosignals. 2009; 17:242–254. [PubMed: 19816061]

Placzek M, Briscoe J. The floor plate: multiple cells, multiple signals. Nat Rev Neurosci. 2005; 6:230–240. [PubMed: 15738958]

Poncet C, Soula C, Trousse F, Kan P, Hirsinger E, Pourquie O, Duprat AM, Cochard P. Induction of oligodendrocyte progenitors in the trunk neural tube by ventralizing signals: effects of notochord and floor plate grafts, and of sonic hedgehog. Mech Dev. 1996; 60:13–32. [PubMed: 9025058]

Postlethwait J, Amores A, Cresko W, Singer A, Yan YL. Subfunction partitioning, the teleost radiation and the annotation of the human genome. Trends Genet. 2004; 20:481–490. [PubMed: 15363902]

Postlethwait JH. The zebrafish genome in context: ohnologs gone missing. J Exp Zool B Mol Dev Evol. 2007; 308:563–577. [PubMed: 17068775]

Pradere JP, Tarnus E, Gres S, Valet P, Saulnier-Blache JS. Secretion and lysophospholipase D activity of autotaxin by adipocytes are controlled by N-glycosylation and signal peptidase. Biochim Biophys Acta. 2007; 1771:93–102. [PubMed: 17208043]

Pringle NP, Richardson WD. A singularity of PDGF alpha-receptor expression in the dorsoventral axis of the neural tube may define the origin of the oligodendrocyte lineage. Development. 1993; 117:525–533. [PubMed: 8330523]

Pringle NP, Yu WP, Guthrie S, Roelink H, Lumsden A, Peterson AC, Richardson WD. Determination of neuroepithelial cell fate: induction of the oligodendrocyte lineage by ventral midline cells and sonic hedgehog. Dev Biol. 1996; 177:30–42. [PubMed: 8660874]

Richardson WD, Kessaris N, Pringle N. Oligodendrocyte wars. Nat Rev Neurosci. 2006; 7:11–18. [PubMed: 16371946]

Richardson WD, Smith HK, Sun T, Pringle NP, Hall A, Woodruff R. Oligodendrocyte lineage and the motor neuron connection. Glia. 2000; 29:136–142. [PubMed: 10625331]

Rinner O, Makhankov YV, Biehlmaier O, Neuhauss SC. Knockdown of cone-specific kinase GRK7 in larval zebrafish leads to impaired cone response recovery and delayed dark adaptation. Neuron. 2005; 47:231–242. [PubMed: 16039565]

Robu ME, Larson JD, Nasevicius A, Beiraghi S, Brenner C, Farber SA, Ekker SC. p53 activation by knockdown technologies. PLoS Genet. 2007; 3:e78. [PubMed: 17530925]

Rowitch DH. Glial specification in the vertebrate neural tube. Nat Rev Neurosci. 2004; 5:409–419. [PubMed: 15100723]

Rowitch DH, Kriegstein AR. Developmental genetics of vertebrate glial-cell specification. Nature. 2010; 468:214–222. [PubMed: 21068830]

Rowitch DH, Lu QR, Kessaris N, Richardson WD. An 'oligarchy' rules neural development. Trends Neurosci. 2002; 25:417–422. [PubMed: 12127759]

Samadi N, Bekele R, Capatos D, Venkatraman G, Sariahmetoglu M, Brindley DN. Regulation of lysophosphatidate signaling by autotaxin and lipid phosphate phosphatases with respect to tumor progression, angiogenesis, metastasis and chemo-resistance. Biochimie. 2011; 93:61–70. [PubMed: 20709140]

Saunders LP, Cao W, Chang WC, Albright RA, Braddock DT, De La Cruz EM. Kinetic analysis of Autotaxin reveals substrate-specific catalytic pathways and a mechanism for lysophosphatidic acid distribution. J Biol Chem. 2011; 286:30130–30141. [PubMed: 21719699]

Sayers EW, Barrett T, Benson DA, Bolton E, Bryant SH, Canese K, Chetvernin V, Church DM, DiCuccio M, Federhen S, et al. Database resources of the National Center for Biotechnology Information. Nucleic Acids Res. 2011; 39(Database issue):D38–D51. [PubMed: 21097890]

Schebesta M, Serluca FC. olig1 expression identifies developing oligodendrocytes in zebrafish and requires hedgehog and notch signaling. Dev Dyn. 2009; 238:887–898. [PubMed: 19253391]

Seiler C, Finger-Baier KC, Rinner O, Makhankov YV, Schwarz H, Neuhauss SC, Nicolson T. Duplicated genes with split functions: independent roles of protocadherin15 orthologues in zebrafish hearing and vision. Development. 2005; 132:615–623. [PubMed: 15634702]

Skokal, RR.; Rohlf, FJ., editors. Biometry: the principle and practice in biological research. 3d ed.. New York: W. H. Freeman and Company; 1995.

Stainier DY. Zebrafish genetics and vertebrate heart formation. Nat Rev Genet. 2001; 2:39–48. [PubMed: 11253067]

Stankoff B, Barron S, Allard J, Barbin G, Noel F, Aigrot MS, Premont J, Sokoloff P, Zalc B, Lubetzki C. Oligodendroglial expression of Edg-2 receptor: developmental analysis and pharmacological responses to lysophosphatidic acid. Mol Cell Neurosci. 2002; 20:415–428. [PubMed: 12139919]

Strahle U, Blader P, Henrique D, Ingham PW. Axial, a zebrafish gene expressed along the developing body axis, shows altered expression in cyclops mutant embryos. Genes Dev. 1993; 7:1436–1446. [PubMed: 7687227]

Sussman CR, Dyer KL, Marchionni M, Miller RH. Local control of oligodendrocyte development in isolated dorsal mouse spinal cord. J Neurosci Res. 2000; 59:413–420. [PubMed: 10679778]

Svetlov SI, Ignatova TN, Wang KK, Hayes RL, English D, Kukekov VG. Lysophosphatidic acid induces clonal generation of mouse neurospheres via proliferation of Sca-1- and AC133-positive neural progenitors. Stem Cells Dev. 2004; 13:685–693. [PubMed: 15684836]

Takada N, Appel B. Identification of genes expressed by zebrafish oligodendrocytes using a differential microarray screen. Dev Dyn. 2010; 239:2041–2047. [PubMed: 20549738]

Takebayashi H, Nabeshima Y, Yoshida S, Chisaka O, Ikenaka K. The basic helix-loop-helix factor olig2 is essential for the development of motoneuron and oligodendrocyte lineages. Curr Biol. 2002; 12:1157–1163. [PubMed: 12121626]

Tanaka M, Okudaira S, Kishi Y, Ohkawa R, Iseki S, Ota M, Noji S, Yatomi Y, Aoki J, Arai H. Autotaxin stabilizes blood vessels and is required for embryonic vasculature by producing lysophosphatidic acid. J Biol Chem. 2006; 281:25822–25830. [PubMed: 16829511]

Taylor JS, Braasch I, Frickey T, Meyer A, Van de Peer Y. Genome duplication, a trait shared by 22000 species of ray-finned fish. Genome Res. 2003; 13:382–390. [PubMed: 12618368]

Thisse C, Thisse B. High-resolution in situ hybridization to whole-mount zebrafish embryos. Nat Protoc. 2008; 3:59–69. [PubMed: 18193022]

Tokumura A, Majima E, Kariya Y, Tominaga K, Kogure K, Yasuda K, Fukuzawa K. Identification of human plasma lysophospholipase D, a lysophosphatidic acid-producing enzyme, as autotaxin, a multifunctional phosphodiesterase. J Biol Chem. 2002; 277:39436–39442. [PubMed: 12176993]

Trevarrow B, Marks DL, Kimmel CB. Organization of hindbrain segments in the zebrafish embryo. Neuron. 1990; 4:669–679. [PubMed: 2344406]

Ulrich F, Ma LH, Baker RG, Torres-Vazquez J. Neurovascular development in the embryonic zebrafish hindbrain. Dev Biol. 2011; 357:134–151. [PubMed: 21745463]

Umezu-Goto M, Kishi Y, Taira A, Hama K, Dohmae N, Takio K, Yamori T, Mills GB, Inoue K, Aoki J, et al. Autotaxin has lysophospholipase D activity leading to tumor cell growth and motility by lysophosphatidic acid production. J Cell Biol. 2002; 158:227–233. [PubMed: 12119361]

Vallstedt A, Klos JM, Ericson J. Multiple dorsoventral origins of oligodendrocyte generation in the spinal cord and hindbrain. Neuron. 2005; 45:55–67. [PubMed: 15629702]

van der Sar AM, Zivkovic D, den Hertog J. Eye defects in receptor protein-tyrosine phosphatase alpha knock-down zebrafish. Dev Dyn. 2002; 223:292–297. [PubMed: 11836793]

van Meeteren LA, Moolenaar WH. Regulation and biological activities of the autotaxin-LPA axis. Prog Lipid Res. 2007; 46:145–160. [PubMed: 17459484]

van Meeteren LA, Ruurs P, Stortelers C, Bouwman P, van Rooijen MA, Pradere JP, Pettit TR, Wakelam MJ, Saulnier-Blache JS, Mummery CL, et al. Autotaxin, a secreted lysophospholipase D, is essential for blood vessel formation during development. Mol Cell Biol. 2006; 26:5015–5022. [PubMed: 16782887]

Waskiewicz AJ, Rikhof HA, Hernandez RE, Moens CB. Zebrafish Meis functions to stabilize Pbx proteins and regulate hindbrain patterning. Development. 2001; 128:4139–4151. [PubMed: 11684652]

Weiner JA, Hecht JH, Chun J. Lysophosphatidic acid receptor gene vzg-1/lpA1/edg-2 is expressed by mature oligodendrocytes during myelination in the postnatal murine brain. J Comp Neurol. 1998; 398:587–598. [PubMed: 9717712]

Wu S, Wu Y, Capecchi MR. Motoneurons and oligodendrocytes are sequentially generated from neural stem cells but do not appear to share common lineage-restricted progenitors in vivo. Development. 2006; 133:581–590. [PubMed: 16407399]

Yanagida K, Ishii S. Non-Edg family LPA receptors: the cutting edge of LPA research. J Biochem. 2011; 150:223–232. [PubMed: 21746769]

Yu N, Lariosa-Willingham KD, Lin FF, Webb M, Rao TS. Characterization of lysophosphatidic acid and sphingosine-1-phosphate-mediated signal transduction in rat cortical oligodendrocytes. Glia. 2004; 45:17–27. [PubMed: 14648542]

Yuelling LM, Fuss B. Autotaxin (ATX): a multi-functional and multi-modular protein possessing enzymatic lysoPLD activity and matricellular properties. Biochim Biophys Acta. 2008; 1781:525–530. [PubMed: 18485925]

Yukiura H, Hama K, Nakanaga K, Tanaka M, Asaoka Y, Okudaira S, Arima N, Inoue A, Hashimoto T, Arai H, et al. Autotaxin regulates vascular development via multiple lysophosphatidic acid (LPA) receptors in zebrafish. J Biol Chem. 2011; 286:43972–43983. [PubMed: 21971049]

Zannino DA, Appel B. Olig2+ precursors produce abducens motor neurons and oligodendrocytes in the zebrafish hindbrain. J Neurosci. 2009; 29:2322–2333. [PubMed: 19244509]

Zhou Q, Anderson DJ. The bHLH transcription factors OLIG2 and OLIG1 couple neuronal and glial subtype specification. Cell. 2002; 109:61–73. [PubMed: 11955447]

A

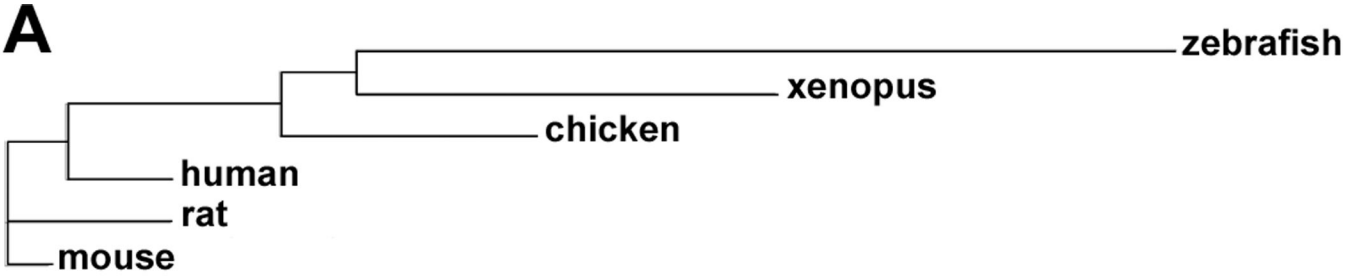

B

	zebrafish	xenopus	chicken	human	rat	mouse
zebrafish		65	66	66	63	66
xenopus			80	76	73	77
chicken				84	80	84
human					90	94
rat						94
mouse						

Fig. 1.

A conserved ortholog to mammalian *atx* exists in the zebrafish. **A:** Guide tree depicting evolutionary sequence relationships between known vertebrate Atx proteins. **B:** Identity table depicting amino acid sequence identities between known vertebrate Atx proteins. For Ensembl transcript IDs see Fig. S1.

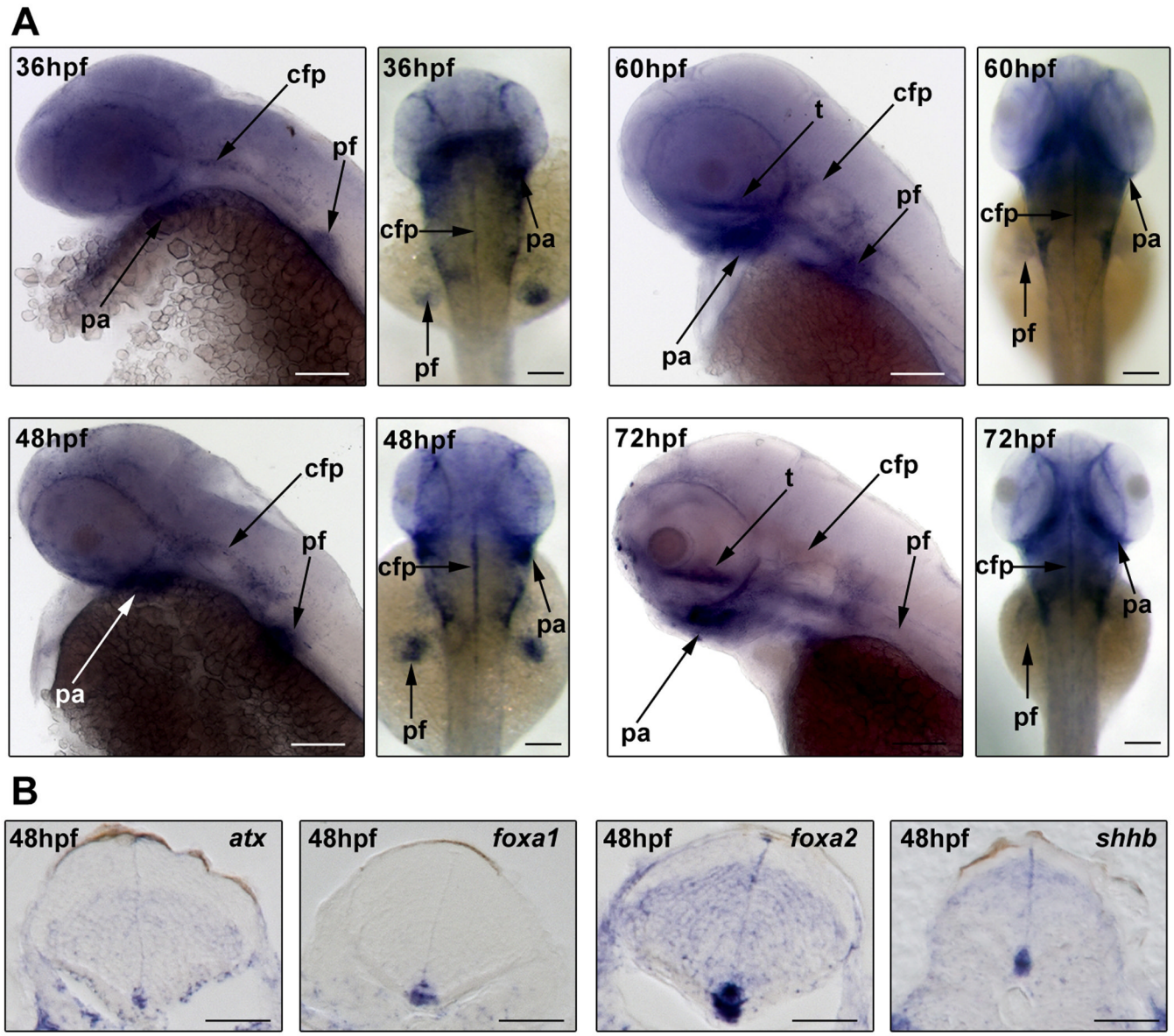

Fig. 2.

During zebrafish development *atx* is expressed in a pattern that includes a prominent expression in the ventral CNS. Embryos were collected at different developmental ages and analyzed by whole-mount *in situ* hybridization. **A**: Representative images of whole-mount embryos *in situ* hybridized for *atx*. Developmental ages are noted in hours post fertilization (hpf). Left panels for each developmental age depict lateral views, anterior is to the left. Right panels depict dorsal views, anterior is to the top. pharyngeal arches (pa), pectoral fin buds (pf), cephalic floor plate (cfp) and trabeculae cranii (t). Scale bars: 100 μm. **B:** Representative images of transverse sections through the hindbrain of 48 hpf embryos. Dorsal is to the top. cephalic floor plate markers (*foxa1*, *foxa2*, *shhb*). Scale bars: 50 μm

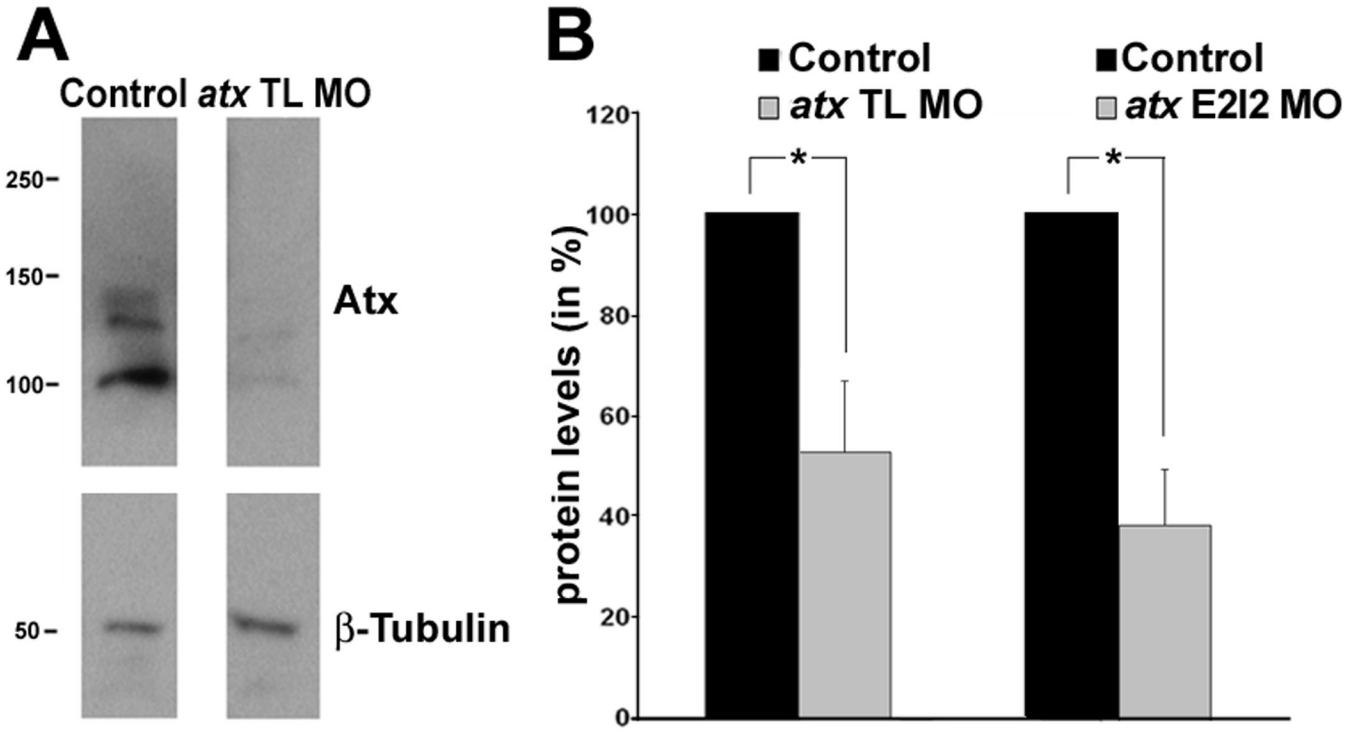

Fig. 3.

Injection of anti-*atx* morpholino oligonucleotides leads to a significant reduction in Atx protein levels. Embryos were injected with either an anti-*atx* translation blocking (*atx* TL MO) or an anti-*atx* splice site targeted (*atx* E2I2 MO) morpholino oligonucleotide and analyzed at 48 hpf. As controls, 5 base pair mismatch morpholino oligonucleotides were used. **A:** Representative Western blot depicting Atx protein levels. β-tubulin was used for normalization. Numbers on the left indicate molecular weights in kD. Protein forms with apparent molecular weights of 100 kD and 125/135 kD were detected and are most likely a result of differences in posttranslational modifications (Jansen et al., 2007; Pradere et al., 2007). **B:** Bar graphs depicting Atx protein levels as % of control (control = 100%). The graphs depict three independent experiments. Means and standard errors are shown. Stars indicate an overall significance level of $p<0.05$ (one-sample *t*-test).

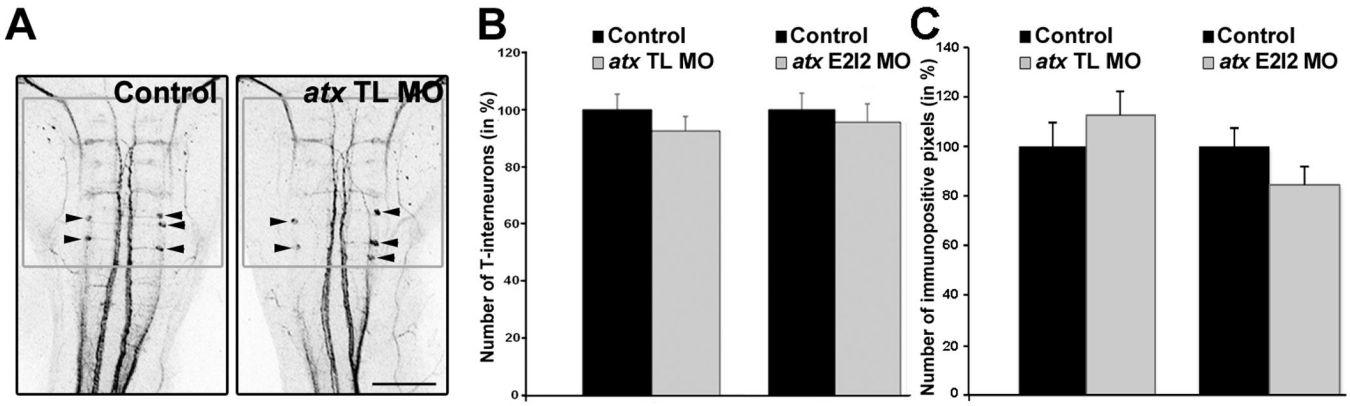

Fig. 4.

In the developing hindbrain knock-down of *atx* expression does not affect neuronal/axonal organization. Embryos were treated as described in Fig. 3 and analyzed at 48 hpf. **A:** Representative images of embryos after whole-mount immnuostaining with the RMO44 antibody. Images represent 2D maximum projections of stacks of 5.66 μm optical sections. Arrowheads point toward T-interneurons. The gray boxes indicate the area used to determine the number of RMO44-immuno-positive pixels. Scale bar: 100 μm. **B–C:** Bar graphs depicting the number of RMO44-immuno-positive T-interneurons (**B**) and pixels (**C**) in % (control = 100%). Means and standard errors of three independent experiments are shown. Student's *t*-test revealed no statistically significant differences.

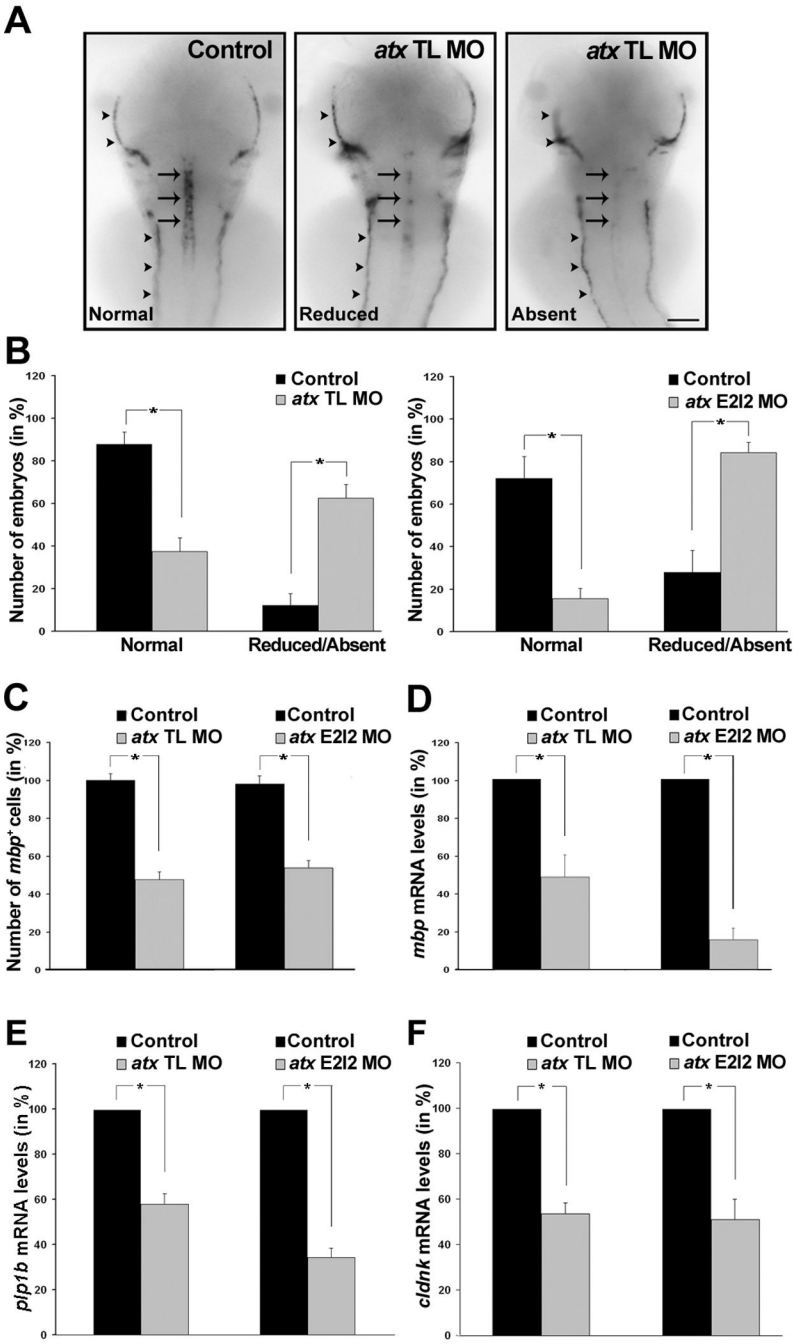

Fig. 5.

In the developing hindbrain knock-down of *atx* expression leads to a reduction in the number of differentiating oligodendrocytes and in the mRNA levels of oligodendrocyte-enriched genes. Embryos were treated as described in Fig. 3 and analyzed at 66 hpf. **A:** Representative images of embryos after whole-mount *in situ* hybridization with a probe specific for *myelin basic protein* (*mbp*). Expression of *mbp* in oligodendrocytes (arrows) was classified into three categories (normal, reduced and absent). Expression of *mbp* in the anterior and posterior lateral line is marked by arrowheads. Dorsal views are shown, anterior is to the top. Scale bar: 100 μm. **B:** Bar graphs depicting the number of embryos with normal or reduced/absent *mbp* mRNA expression in % (total number of embryos per condition =

100%). Means and standard errors of five (left graph) and four (right graph) independent experiments are shown. Stars indicate an overall two-tailed significance level of $p<0.05$ (Student's *t*-test). **C:** Bar graphs depicting the number of *mbp*-positive oligodendrocytes in % (control = 100%). Means and standard errors of four independent experiments are shown. Stars indicate an overall two-tailed significance level of $p<0.05$ (Student's *t*-test). **D–F:** Bar graphs depicting mRNA levels in % (control = 100%) as determined by quantitative RT-PCR for *mbp* (**D**), *proteolipid protein* (*plp1b*) (**E**) and *claudin K* (*cldnk*) (**F**). Means and standard errors of three independent experiments are shown. Stars indicate an overall significance level of $p<0.05$ (one sample *t*-test).

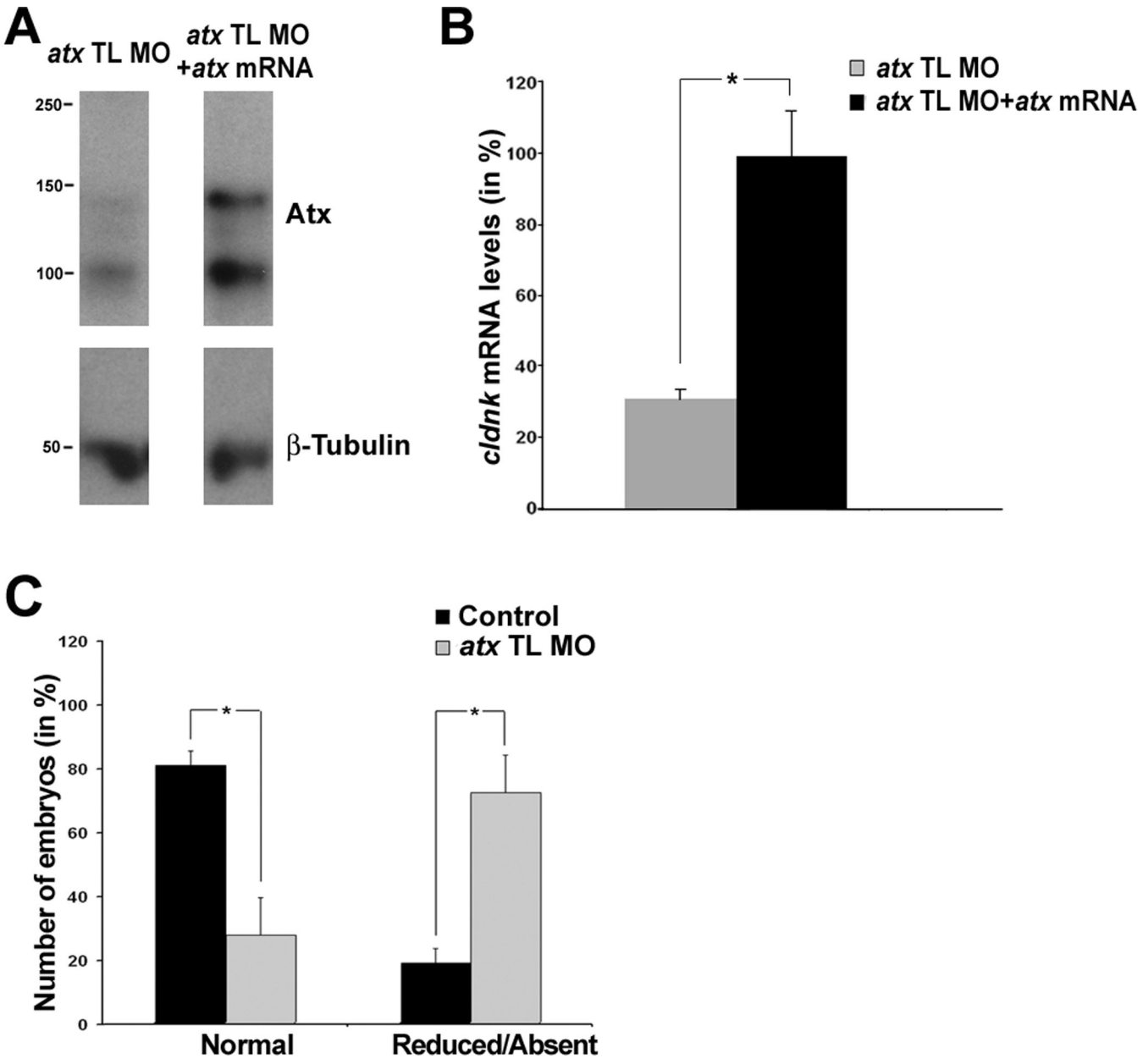

Fig. 6.

Co-injection of a synthetic *atx* mRNA leads to a rescue of the *atx* knock-down phenotype, and there is no apparent recovery from the *atx* knock-down-induced phenotype up to 72 hpf. **A–B:** Embryos were co-injected with *atx* TL MO and a synthetic *atx* mRNA and then analyzed at 48 hpf. As control, a 5 base pair mismatch morpholino oligonucleotide was used. **A:** Representative Western blot depicting Atx protein levels. **β**-tubulin was used for normalization. Numbers on the left indicate molecular weights in kD. **B:** Bar graph depicting *cldnk* mRNA levels in % (control = 100%) as determined by quantitative RT-PCR. Means and standard errors of four independent experiments are shown. The star indicates an overall two-tailed significance level of $p<0.05$ (Student's *t*-test). No statistically significant difference in *cldnk* mRNA level was found between embryos injected with control MO versus *atx* TL MO plus *atx* mRNA (not shown). **C**: Embryos were treated as described in Fig. 3 and analyzed at 72 hpf. The bar graph depicts the number of embryos

with normal or reduced/absent *mbp* mRNA expression in % (total number of embryos per condition = 100%). Means and standard errors of four independent experiments are shown. Stars indicate an overall two-tailed significance level of $p<0.05$ (Student's *t*-test).

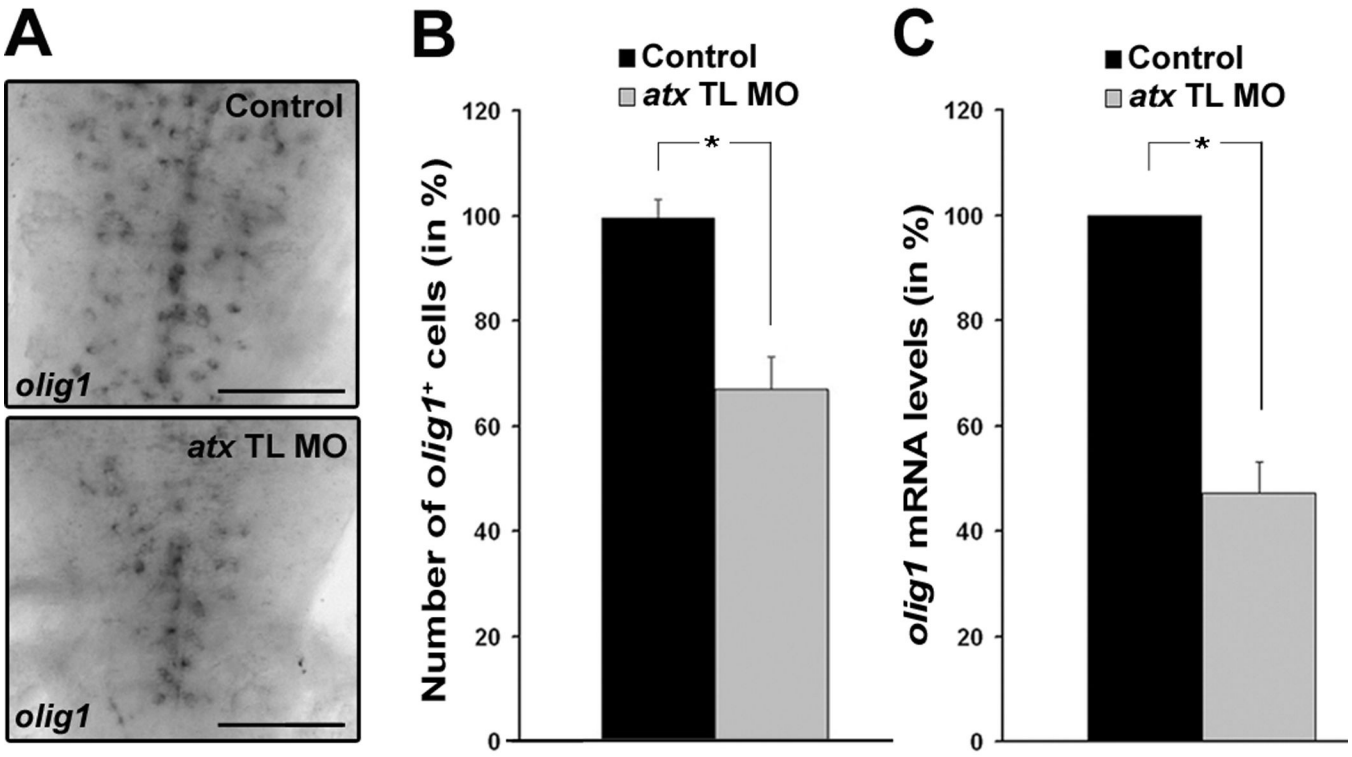

Fig. 7.

In the developing hindbrain knock-down of *atx* expression leads to a reduction in the number of *olig1*-positive cells and the levels of *olig1* mRNA. Embryos were treated as described in Fig. 3 and analyzed at 66 hpf. **A:** Representative images of embryos after whole-mount *in situ* hybridization with a probe specific for *olig1*. Scale bar: 100 μm. **B:** Bar graph depicting the number of *olig1*-positive oligodendrocytes in % (control = 100%). Means and standard errors of three independent experiments are shown. Stars indicate an overall two-tailed significance level of $p<0.05$ (Student's *t*-test). **C:** Bar graph depicting *olig1* mRNA levels in % (control = 100%) as determined by quantitative RT-PCR. Means and standard errors of three independent experiments are shown. Stars indicate an overall significance level of $p<0.05$ (one sample *t*-test).

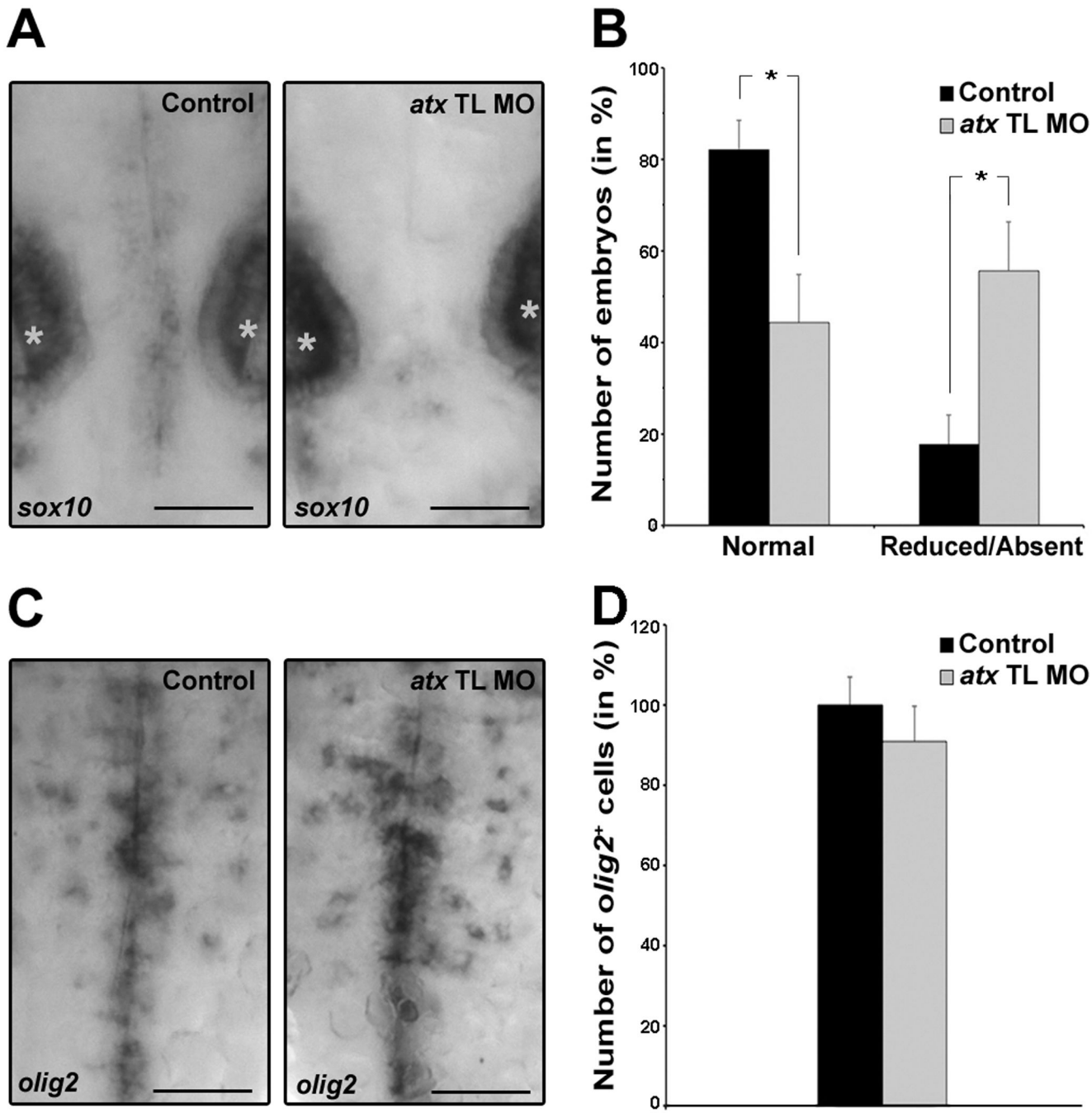

Fig. 8.

In the developing hindbrain knock-down of *atx* expression leads to a reduction in the number of *sox10*-positive but not *olig2*-positive cells. Embryos were treated as described in Fig. 3 and analyzed at 48 hpf. **A:** Representative images of embryos after whole-mount *in situ* hybridization with a probe specific for *sox10*. Stars indicate otic vesicles. Scale bar: 50 μm. **B:** Bar graph depicting the number of embryos with normal (>2 *sox10*-positive cells) or reduced/absent (≤2 *sox10*-positive cells) *sox10* expression in % (total number of embryos per condition = 100%). Means and standard errors of six independent experiments are shown. Stars indicate an overall two-tailed significance level of $p<0.05$ (Student's *t*-test). **C:**

Representative images of embryos after whole-mount *in situ* hybridization with a probe specific for *olig2*. Scale bar: 50 μm. **D:** Bar graph depicting the number of *olig2*-positive oligodendrocytes in % (control = 100%). Means and standard errors of three independent experiments are shown. Student's *t*-test revealed no statistically significant difference.

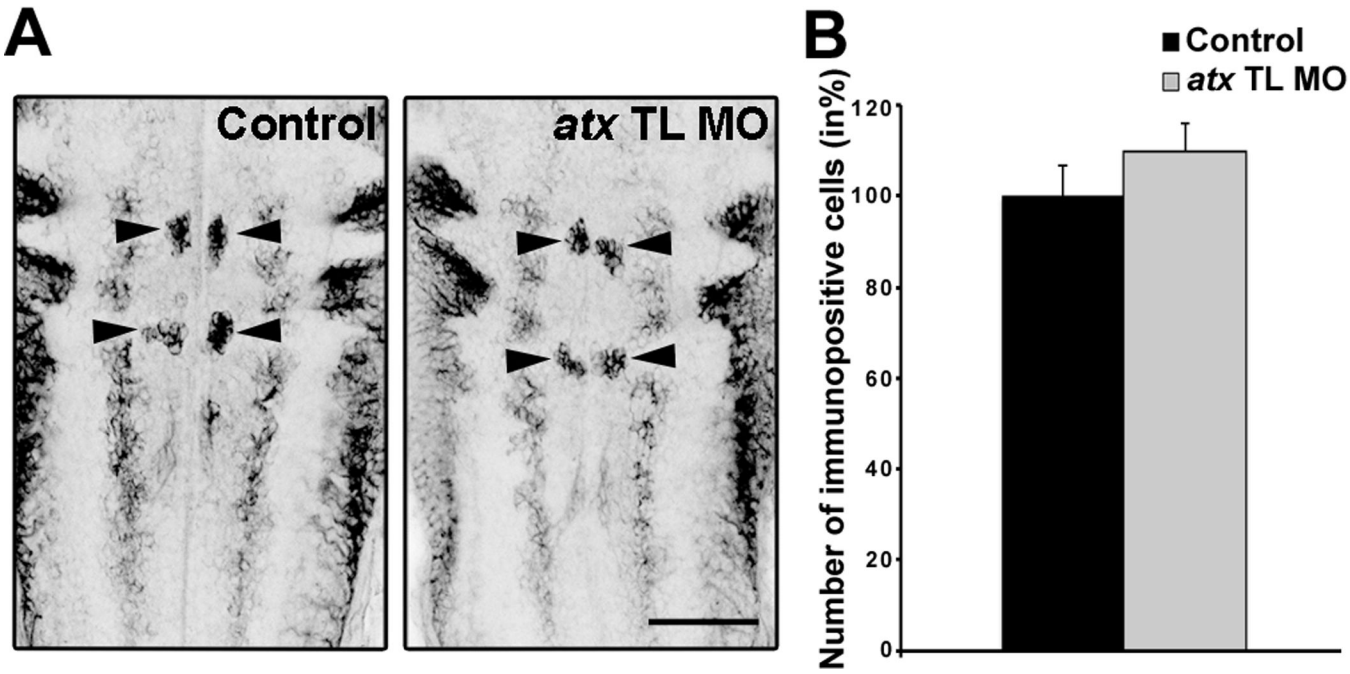

Fig. 9.

In the developing hindbrain knock-down of *atx* expression does not affect the number of somatic abducens motor neurons. Embryos were treated as described in Fig. 3 and analyzed at 48 hpf. **A:** Representative images of embryos after whole-mount immunostaining with the Zn-8 antibody. Images represent 2D maximum projections of stacks of 0.87 μm optical sections. Arrows point toward somatic abducens motor neurons. Zn-8-immuno-positive hindbrain commissural axons are only partially captured. Scale bar: 50 μm. **B:** Bar graph depicting the number of Zn-8-immuno-positive somatic abducens motor neurons in % (control = 100%). Means and standard errors of three independent experiments are shown. Student's *t*-test revealed no statistically significant difference.